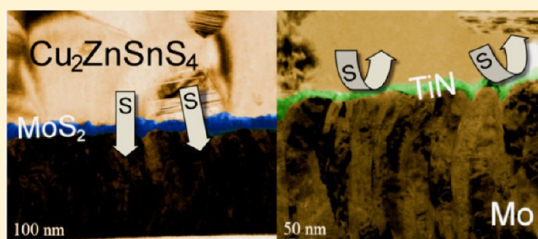


Effects of Back Contact Instability on $\text{Cu}_2\text{ZnSnS}_4$ Devices and ProcessesJonathan J. Scragg,^{*,†} Tomas Kubart,[†] J. Timo Wätjen,[†] Tove Ericson,[†] Margareta K. Linnarsson,[‡] and Charlotte Platzer-Björkman[†][†]Ångström Solar Center, Solid State Electronics, Uppsala University, Box 534, SE-751 21 Uppsala, Sweden[‡]School of Information and Communication Technology, Integrated Devices and Circuits, KTH Royal Institute of Technology, Electrum 229, SE-164 40 Kista, Sweden

ABSTRACT: $\text{Cu}_2\text{ZnSnS}_4$ (CZTS) is a promising material for thin film solar cells based on sustainable resources. This paper explores some consequences of the chemical instability between CZTS and the standard Mo “back contact” layer used in the solar cell. Chemical passivation of the back contact interface using titanium nitride (TiN) diffusion barriers, combined with variations in the CZTS annealing process, enables us to isolate the effects of back contact chemistry on the electrical properties of the CZTS layer that result from the synthesis, as determined by measurements on completed solar cells. It is found that instability in the back contact is responsible for large current losses in the finished solar cell, which can be distinguished from other losses that arise from instabilities in the surface of the CZTS layer during annealing. The TiN-passivated back contact is an effective barrier to sulfur atoms and therefore prevents reactions between CZTS and Mo. However, it also results in a high series resistance and thus a reduced fill factor in the solar cell. The need for high chalcogen pressure during CZTS annealing can be linked to suppression of the back contact reactions and could potentially be avoided if better inert back contacts were to be developed.

KEYWORDS: CZTS, kesterite, chalcogenide, thin film, solar cell, interface



INTRODUCTION

The promise of efficient thin film solar cells based on kesterite ($\text{Cu}_2\text{ZnSn}(\text{S},\text{Se})_4$, or CZTS(e)) has inspired a huge amount of research activity because of the potential advantages of low materials cost and abundant resources. Today, the best lab-scale CZTS(e)-based device has a power conversion efficiency of 11.1%,¹ which is indeed promising but is still rather far from the level needed for commercialization. Much of the present literature is devoted to optimization of the many and varied processes used to produce CZTS(e) films (for a review of these, we refer the reader elsewhere^{2,3}) which has led to the gradual improvement of device performance. Meanwhile, an understanding is beginning to emerge of the underlying processes that control material quality from a given synthesis process, in other words, the fundamental chemical properties of the CZTS(e) materials system in the context of the solar cell synthesis. One of the clearest trends to have arisen so far is the need for “two-stage” processing, i.e., separation of the film deposition and heat-treatment steps in film growth. All of the best CZTS(e) devices have come from such processes^{1,4–7,a} This separation of steps is needed because high S(e) partial pressures are required whenever CZTS(e) is processed at high temperature (500–600 °C), whereas the actual film deposition cannot typically be carried out under the same conditions. One way out of this would be to lower the process temperature, which reduces the required S(e) pressure because of the exponential nature of vapor pressure vs temperature curves.

However, this is inherently a compromise, since temperature is important for other aspects of synthesis, such as grain growth and diffusion.

On the basis of the current understanding, the high chalcogen pressure during thermal processing is needed to suppress decomposition reactions of CZTS(e) that can occur at the high temperatures of synthesis. Some important examples are summarized in Table 1 for the sulfide case, although the selenide case is expected to be very similar. Reaction 1 is the thermal decomposition of CZTS, first suggested by Weber⁹ as the cause of Sn losses (by evaporation of SnS) during heating. It has been proposed that this reaction is the main reason that CZTS is unstable at high temperatures in the absence of chalcogen excess.¹³ Table 1 also shows two related reactions 2 and 3 that may occur at the film surface depending on the presence of the secondary phases SnS_2 and Sn_2S_3 prior to or during CZTS formation. The reason that reactions 1–3 occur is that Sn–S bonds are too weak to resist the entropic gain from vaporization of S, which has a very high vapor pressure at normal annealing temperatures.¹² The shared characteristics of reactions 1–3 are (a) that they occur at the film surface, (b) that they cause loss of S and SnS from the CZTS film, and (c) that they are suppressed by the presence of S and SnS

Received: May 8, 2013

Revised: June 27, 2013

Published: July 2, 2013

Table 1. Known and Inferred Reactions Occurring at the Surface and Back Contact of CZTS Films during Annealing

| surface reactions | | ref |
|---|-----|----------|
| $2\text{Cu}_2\text{ZnSnS}_4 \rightleftharpoons \text{Cu}_2\text{S} + \text{ZnS} + \text{SnS}(s/g) + (1/2)\text{S}_2(g)$ | (1) | 8, 9 |
| $2\text{SnS}_2 \rightleftharpoons \text{Sn}_2\text{S}_3 + (1/2)\text{S}_2(g)$ | (2) | 10 |
| $\text{Sn}_2\text{S}_3 \rightleftharpoons 2\text{SnS}(g) + (1/2)\text{S}_2(g)$ | (3) | 10 |
| back contact reactions | | source |
| $2\text{CZTS} + \text{Mo} \rightarrow 2\text{Cu}_2\text{S} + 2\text{ZnS} + 2\text{SnS} + \text{MoS}_2$ | (4) | 11 |
| $2\text{SnS}_2 + \text{Mo} \rightarrow 2\text{SnS} + \text{MoS}_2$ | (5) | 12 |
| $2\text{Sn}_2\text{S}_3 + \text{Mo} \rightarrow 2\text{SnS} + 2\text{MoS}_2$ | (6) | inferred |
| $\text{Mo} + \text{S}_2(g) \rightarrow \text{MoS}_2$ | (7) | 12 |

Table 2. Samples Referred to in This Study, Indicating the Back Contact Type, Anneal Method, and the Approximate Chemical Stability of the Surface and Back Contact Interfaces during Annealing, According to the Chemical Reactions Described in Table 1^a

| sample | back contact type | anneal method | surface condition | back contact condition | Cu/Sn | Cu/Zn | r_s |
|--------|-------------------|------------------|----------------------|------------------------|-------|-------|-------|
| A | SLG/Mo | graphite box + S | stable | ~stable ^b | 2.0 | 1.9 | 0.99 |
| B | SLG/Mo/TiN | graphite box + S | stable | stable | 2.0 | 1.9 | 1.0 |
| C | SLG/Mo | glass cover | ~stable ^c | unstable | 2.0 | 1.9 | 1.0 |
| D | SLG/Mo/TiN | glass cover | ~stable | stable | 2.0 | 1.9 | 1.0 |
| E | SLG/Mo | open box | unstable | unstable | 2.0 | 1.8 | 1.0 |
| F | SLG/Mo/TiN | open box | unstable | stable | 2.0 | 1.9 | 1.0 |

^aThe compositions shown are from EDS measurements. $r_s = S/(0.5\text{Cu} + \text{Zn} + 2\text{Sn})$, where S, Cu, Zn, and Sn are the EDS atomic fractions (see Experimental Section for explanation). ^bAlthough the Mo/CZTS back contact interface is *initially* unstable, it gets rapidly stabilized by the formation of MoS_2 at the interface because of the supplied S excess, and any damage to the CZTS layer may be subsequently “healed” by the S excess.¹¹ ^cThe glass cover is not completely effective in stabilizing the surface because of the fact that it does not form a truly closed system above the CZTS surface; i.e., there are openings at the edges of the sample.

vapors.^{8,13} In ref 8 it was shown that reaction 1 causes large losses in device performance in both voltage and current.

Recently, another decomposition process was shown to occur at the interface between CZTS and the normal “back contact” material, Mo, at the high temperatures used in synthesis.¹¹ This is shown as reaction 4 in Table 1. It is driven by the energetically favorable formation of MoS_2 , which outweighs the cost of decomposing the CZTS lattice, and again can be traced back to the weakness of Sn–S bonds.^{11,12} We can again expect similar reactions between Mo and SnS_2 or Sn_2S_3 , if present, i.e., reactions 5 and 6 in Table 1. Such solid-state interface reactions can be self-limiting if the accumulation of reaction products at the interface creates a barrier to further reaction. For this reason, it was suggested that an external pressure of S vapor, by causing rapid formation of MoS_2 (reaction 7 in Table 1), should suppress further reactions between Mo and the CZTS layer, assuming that the MoS_2 layer becomes thick enough to effectively prevent diffusion of S atoms on the time scale of the heat treatment.¹¹

It is not yet known whether the back contact reactions have any adverse effects on the electrical properties of the CZTS layer, i.e., whether they impact on device performance. However, the fact that the back contact reactions also depend strongly on S pressure during heat treatment challenges the current understanding that the need for high S pressures to make good quality material is only due to the surface reactions. The aim of this study is thus to determine if the back contact decomposition reactions are also limiting the device-relevant qualities of the material, i.e., whether they are significant in the optimization of synthetic strategies for CZTS (or, more generally, CZTS(e)). A key requirement for carrying out this study was to develop an alternative, chemically inert back

contact in order to separate the effects of surface and back contact chemistry. We achieved this using a thin layer of the chemically inert conductor titanium nitride (TiN), which we show can effectively passivate the Mo/CZTS interface. By use of device characterization as the primary means of detecting changes in the CZTS layer properties, deliberate variations in the anneal process coupled with the modified back contacts enabled us to clearly distinguish between performance losses that must originate from the surface chemistry and those that must originate from the back contact chemistry during annealing. In particular, we show that one of the key functions of S vapor during annealing is suppression of a detrimental back contact process that causes severe current losses in finished solar cells.

EXPERIMENTAL SECTION

Two kinds of back contacts were produced in this study: unmodified Mo back contacts of approximately 350 nm thickness and passivated back contacts that consisted of the same Mo layer coated with 10–20 nm of titanium nitride (TiN). The Mo layers were prepared by dc sputtering onto clean soda lime glass (SLG) substrates, as described previously.¹⁴ The TiN layers were deposited using reactive sputtering in a Von Ardenne CS 730S system. A Ti target (99.99%) was sputtered in a flow of 8 sccm nitrogen (99.9995%) and 40 sccm argon (99.9997%), at a sputter pressure of 6 mTorr. The bulk resistivity of the TiN was calculated from the sheet resistance measured on 25 mm × 25 mm samples of 1 μm thickness using a 4-point probe (AIT model CMT-SR2000N).

Cu–Zn–Sn–S precursor films were deposited onto these substrates using reactive pulsed dc magnetron cosputtering from Cu/Sn (65:35) alloy and pure Zn targets in an atmosphere of H_2S . The target powers were 560–580 and 540–620 W, respectively, with a pulse frequency of 20 kHz. The base pressure of the system (Von Ardenne CS 600) is below 10^{-4} Pa and the sputtering pressure 0.7 Pa at an H_2S flow rate of

30 sccm. The substrates were heated to approximately 180 °C during deposition. More details can be found in ref 15.

The metallic composition of the precursor films was determined by X-ray fluorescence spectroscopy (XRF, PANalytical Epsilon 5) with calibration samples measured with Rutherford backscattering spectrometry. The sulfur content was measured using a LEO 440 SEM with an energy dispersive X-ray spectroscopy (EDS) system. The CZTS films used for devices in this study were produced from a single sputtering run and were therefore identical. The precursors had metallic composition (as measured by XRF) of Cu/Sn = 1.9 and Cu/Zn = 1.8. The weighted sulfur content based on EDS measurements, $r_s = 2S/(Cu + 2Zn + 4Sn)$, had a value of 1.0.¹⁶ This shows that the precursors can be correctly described as being in the $Cu_2S-ZnS-SnS_2$ phase space to which CZTS belongs¹⁷ and are stoichiometric in sulfur.

The precursor films were annealed in a tube furnace with a central hot zone and an outer water-cooled zone/loading area. In this system, fast heating is achieved by transferring the samples from the cold zone into the hot furnace using a transfer rod. The samples were annealed at 560–570 °C for 10 min in a static anneal atmosphere of 0.3 atm of argon before being withdrawn to the cold zone. The precursors were loaded into the furnace in one of three different configurations, described as follows. The first, which is our “baseline” process for CZTS devices, was to place the samples in a small graphite container (6.5 cm³ internal volume) along with 20 mg of elemental sulfur. In the second anneal configuration, the samples were placed in a heat-cleaned graphite box without adding S, and a glass plate was placed directly on top of them, i.e., in contact with the film surfaces. The third configuration used was to anneal the samples in an open graphite box, with neither the glass cover nor added S. In each of the three configurations, two precursors were annealed together, one with the unmodified Mo back contact and one with the TiN-passivated back contact. Table 2 summarizes the samples referred to in this study.

The composition of the films after annealing was determined by EDS on sample sections prior to device processing. The EDS measurements (for the metal elements) were calibrated using the known metallic compositions of the precursor based on XRF.

Devices were prepared from the annealed CZTS films as follows. First, the films were etched in 5 wt % KCN solution for 2 min. The CdS buffer layer was then deposited using chemical bath deposition, and the window and TCO layers (*i*-ZnO and Al:ZnO) were deposited by sputtering. Finally, Ni/Al/Ni contact grids were applied by e-beam evaporation. All the device finishing processes except for the KCN etch are in the standard Ångström Solar Center baseline, described in more detail elsewhere.¹⁴ Air exposure time was minimized between all steps.

Current–voltage (*J*–*V*) measurements were made under a halogen lamp with a cold mirror. The samples were placed on a temperature controlled stage. External quantum efficiency (EQE) measurements, calibrated using a Hamamatsu Si solar cell, were performed without bias. To reduce errors due to mismatch between the halogen lamp and the AM1.5 spectrum, the intensity of the *J*–*V* lamp was adjusted to obtain the short circuit current density determined by the EQE measurement, after correcting for grid shading (approximately 2.5%).

Analysis of the depth distributions of Na, S, Cu, Zn, Sn, and Mo was made on certain finished devices using secondary ion mass spectrometry (SIMS) utilizing a Cameca ims 4f instrument. A sputter beam of 5.7 keV ³²(O₂)⁺ ions was rastered over an area of 200 × 200 μm², and secondary ions of ²³Na⁺, ³²S⁺, ⁶³Cu⁺, ⁶⁷Zn⁺, ⁹⁸Mo⁺, and ¹²⁰Sn⁺ were collected from the central part of this area (~60 μm in diameter). Energy filtering was employed to minimize interference from molecular ions.

Cross-sectional transmission electron microscopy (TEM) samples were prepared using a focused ion beam (FIB) and a FEI Strata DB232 dual beam and were mounted to Mo grids. A final ion polishing energy of 5 keV was used. A Tecnai F30 ST TEM, equipped with EDS detector and a GIF2002 energy filter, was used for characterization. Elemental profiles were acquired with EDS for Cu, Zn, Sn, Mo, and Ti. As S-K overlaps with Mo-L in EDS, the S-L_{2,3} edge in the electron energy loss spectra (EELS) was used as a measure of the S content using an 10 eV energy window starting at 177 eV. Ti and

N were also measured with EELS in the energy windows 455–466 and 400–414 eV, respectively.

Scanning electron microscopy (SEM) was performed in a LEO 1550 with an in-lens detector. EDS mapping in the same system was carried out with an Oxford Instruments X-Max detector, using an accelerating voltage of 20 keV. The samples were coated with a few nanometers of Au–Pd alloy to prevent charging, and sample drift was compensated in the software.

Raman scattering measurements on as-annealed samples were made using a laser excitation wavelength of 514 nm in a Renishaw system. The spot size was of the order of 10 μm × 10 μm. In certain cases, a “lift-off” method was used to expose the back surfaces of the CZTS layers. Adhesive tape was applied to the film surface, and the film was peeled away with the assistance of a razor blade.

RESULTS AND DISCUSSION

This section consists of three parts. In the first part, we discuss the development of the TiN-passivated back contact for CZTS, including its chemical and electrical properties. In the second part, we compare the device characteristics of the six samples A–F listed in Table 2 to pinpoint the different influences of the surface and back contact decomposition reactions. Finally, we compare materials characterization of the same samples.

Part I: TiN Back Contact. The basic characterization and electrical properties of TiN films prepared in our reactive sputter system have been described elsewhere.¹⁸ We tested the chemical stability of the films under normal CZTS annealing conditions by comparing their Raman spectra (not shown) before and after annealing in sulfur vapor at 560 °C. The peaks seen at around 200, 325, 465, and 553 cm⁻¹ match the literature values for TiN¹⁹ and were not affected by the anneal. There were no indications of decomposition (e.g., peak broadening) or sulfurization (e.g., formation of TiS₂ or TiS₃) in the Raman spectrum, which is consistent with the known inertness of TiN.

Initial attempts to prepare CZTS layers on bulk (~1 μm) TiN back contacts failed because of blocking of Na transport from the glass substrate, which inhibited grain growth in the film and gave poor adhesion. Much better results were obtained by taking our normal Mo-coated glass substrates and depositing a very thin (~20 nm) TiN layer prior to deposition of the CZTS films. This approach has previously been employed in the case of CZTSe, with the intention of preventing aggressive selenisation of Mo during annealing in a Se-rich atmosphere.⁵ When using these thin TiN layers, we found that the CZTS films recrystallized as normal during annealing, and the adhesion was greatly improved.

The SIMS depth profiles in Figure 1 show that the CZTS layers in samples A and B (see Table 2) have almost identical distributions of Cu, Zn, and Sn. There is a possible accumulation of Zn at the back contact in both cases (although the interpretation of SIMS data at interfaces is not certain because of changes in sputtering rate). The right side of Figure 1 shows the Na, S, and Mo profiles for the same samples. We see that the TiN layer had essentially no influence on the Na content and distribution in sample B. The only clear difference between the samples is that the Mo and S signals peak at the back contact interface in sample A, whereas in sample B no peak is seen for either element. This is initial evidence for the presence of a thicker layer of MoS₂ in sample A compared with sample B.

Figure 2a and Figure 2b show cross-sectional SEM images taken at the back contact region in samples A and B, those that were annealed with excess S. In sample A, with no TiN layer,

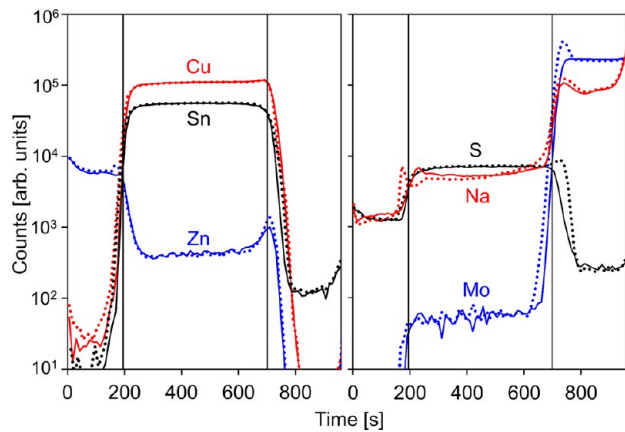


Figure 1. Overlaid SIMS depth profiles for completed devices A (dotted lines) and B (solid lines). Sample B has a TiN layer at the back contact: (left) Cu, Zn, and Sn profiles; (right) Na, S, and Mo profiles. The vertical lines at about 190 and 700 s respectively indicate estimates of the front and back interface locations of the CZTS layers and can be used to compare the left and right plots. The device structure is ZnO/CdS/CZTS ($\sim 2 \mu\text{m}$)/(TiN)/Mo/glass, with the ZnO layer being to the left in the figure.

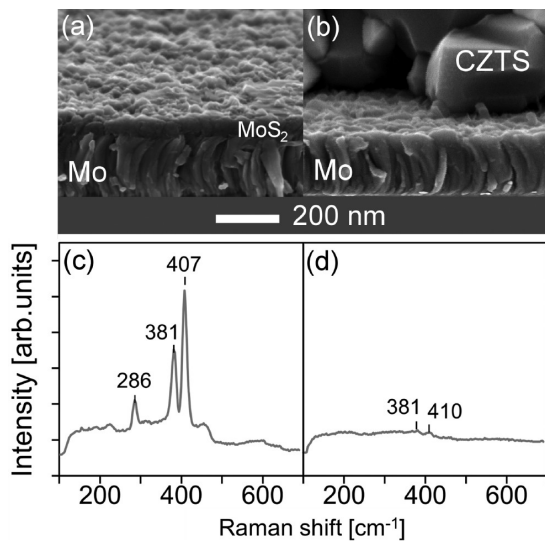


Figure 2. Above: SEM cross section images in the back contact regions of (a) sample A (Mo back contact) and (b) sample B (TiN-coated Mo back contact) after annealing. Areas where the CZTS film had flaked away during sectioning were chosen to more clearly reveal the back contact. Below: Raman spectra of respective back contacts of (c) sample A and (d) sample B after annealing and mechanical removal of the CZTS layers. The indicated peak positions correspond to MoS_2 .

the Mo is covered by an approximately 60–70 nm layer, which was confirmed as MoS_2 by using Raman scattering; strong bands were seen at 407, 381, and 286 cm^{-1} , as in Figure 2c.²⁰ With the TiN layer (sample B), no MoS_2 can be seen by SEM (the TiN layer itself cannot be resolved in this image), and Raman showed only extremely weak bands for MoS_2 (Figure 2d). These differences in MoS_2 thickness between A and B are consistent with the SIMS results. We conclude that even this thin TiN layer is an effective barrier to S atoms, preventing S vapor from reacting with the underlying Mo.

To determine whether the TiN also prevents reactions between Mo and the CZTS layer itself, we examined the back contacts of samples C and D, which were annealed without

added sulfur. Figure 3a and Figure 3b show TEM cross sections of the back contact regions of these samples. With the

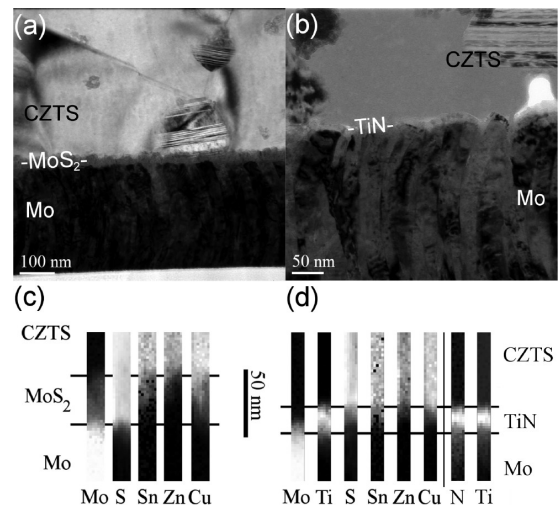


Figure 3. Bright field TEM images of back contacts in (a) sample C, showing MoS_2 layer, and (b) sample D, showing TiN layer. Below: elemental profiles in the back contact regions of (c) sample C and (d) sample D, from EDS (Cu, Zn, Sn, Mo, Ti) and EELS (S, N, Ti) measurements on TEM cross sections.

unmodified back contact (sample C), an approximately 30 nm MoS_2 layer can be seen (the thinner layer reflecting the lower availability of S in this anneal configuration). To confirm that this did not arise from residual S vapor in the annealing system, we annealed a bare Mo piece in the same configuration. In that case, no MoS_2 could be resolved by SEM, and the Raman intensity of MoS_2 peaks was comparable to that in Figure 2d. Thus, the MoS_2 layer seen in Figure 3a must come mainly from the reaction between Mo and the CZTS film. In sample D, Figure 3b, the TiN layer can just be visualized, a 10–20 nm thick, conformal coating on the Mo. Elemental depth profiles from EDS and EELS are shown for samples C and D in Figure 3c and Figure 3d. The MoS_2 in sample C is clear. In sample D, the TiN layer can be seen, and we note that the S concentration below the TiN layer is negligible. In the previous work on TiN barriers for CZTSe films, a mixed TiN/ MoSe_2 layer was found after selenization.⁵ In the present case, the TiN layer remains intact, which may be because of differences in the quality (e.g., uniformity, stoichiometry, or density) of the respective TiN layers or because of differences in the annealing processes for the CZTS(e) films. We can conclude that the thin TiN layers used here almost completely block sulfurization of the underlying Mo, both from an excess S pressure in the annealing atmosphere and crucially from reaction with the CZTS layer itself.

Table 3 shows the device metrics and diode parameters for samples A–F, determined from fitting of the one-diode model to the current voltage (J – V) data using the procedure described by Hegedus and Shafarman.²¹ Since the J – V curves under illumination typically exhibited voltage-dependent carrier collection, we give here only the parameters extracted from the dark curves, which give the more reliable fit to the one-diode model. Sample A represents our baseline CZTS device process, having a standard Mo back contact and being annealed in S vapor excess. The device efficiency of 7.9% is among the better reported efficiencies for pure sulfide CZTS devices at the time

Table 3. Sample Descriptions (Repeated from Table 2 for Clarity), Device Metrics, and Diode Parameters for Samples A–F

| sample | back contact | anneal method | V_{oc} [mV] | J_{sc} [mA cm^{-2}] | FF [%] | η [%] | A | J_0 [mA cm^{-2}] | R_s [$\Omega \text{ cm}^2$] |
|--------|--------------|------------------|---------------|----------------------------------|--------|------------|-----|-------------------------------|---------------------------------|
| A | SLG/Mo | graphite box + S | 667 | 19.6 | 60.0 | 7.9 | 2.3 | 1.1×10^{-4} | 2.0 |
| B | SLG/Mo/TiN | graphite box + S | 621 | 18.7 | 47.1 | 5.5 | 2.6 | 2.8×10^{-4} | 6.9 |
| C | SLG/Mo | glass cover | 596 | 9.24 | 54.9 | 3.0 | 2.5 | 5.8×10^{-4} | 1.9 |
| D | SLG/Mo/TiN | glass cover | 551 | 17.5 | 44.1 | 4.3 | 2.8 | 1.2×10^{-3} | 3.2 |
| E | SLG/Mo | open box | 203 | 3.15 | 50.3 | 0.32 | 1.8 | 2.1×10^{-2} | 1.0 |
| F | SLG/Mo/TiN | open box | 273 | 3.98 | 48.8 | 0.53 | 1.9 | 3.9×10^{-3} | 1.9 |

of writing.^{4,7} Considering that no antireflective coating is employed here, almost the only difference between sample A and the current record pure sulfide CZTS device is the open circuit voltage, 667 mV compared to the 708 mV reported by Kato et al.⁷ Figure 4 shows J – V curves for devices A and B.

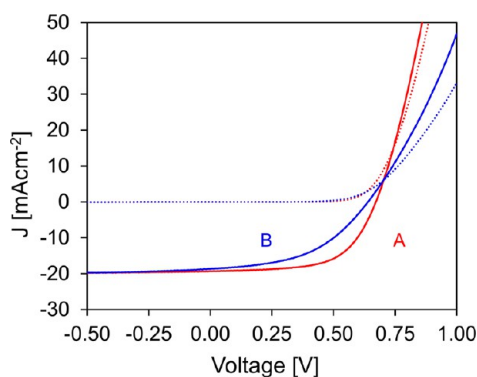


Figure 4. Current–voltage curves for samples A (normal Mo back contact) and B (TiN-passivated Mo back contact), both annealed with S excess.

Sample B is in principle identical to sample A apart from the addition of the TiN barrier. As shown, this did not affect the sodium content of the CZTS layer. However, compared to sample A, we see a large drop in fill factor, from 60% to 47%, mostly related to a dramatic increase in series resistance (from 2.0 to 6.9 $\Omega \text{ cm}^2$). The resulting device efficiency for B is 5.5%, compared to 7.9% for A. In samples A and B, the back contact was in principle chemically stabilized by the presence of excess S during annealing (both samples) and by the presence of the barrier layer (sample B only), so we do not attribute the differences between devices A and B to changes in the CZTS layer at the back contact (this is discussed in more detail below). In addition, the bulk resistivity of the TiN layers, at around 130 $\mu\Omega \text{ cm}$, is far too low to contribute directly to the overall series resistance. In fact, the observed losses in device performance for sample B are similar to those seen when ZrN back contacts are used for CIGS, where it has been suggested that a barrier for majority carriers is formed.²² This resulted in a large increase in contact resistance, contributing to an overall high series resistance and causing losses in fill factor. Additionally, the barrier was supposed to enhance the rate of recombination near the back contact, causing an increase in reverse saturation current density and a drop in the open circuit voltage. All of these effects can be seen in sample B, which suggests the presence of a similar barrier at the TiN/CZTS interface. However, we cannot presently rule out other contributions to the higher series resistance, for example, changes in the CZTS conductivity. In the earlier work on TiN barrier layers (for CZTSe films),⁵ this problem was not so apparent. Although the fill factor of the best device in that study

was low, at 54%, the series resistance was only moderate, at 1.8 $\Omega \text{ cm}^2$. We attribute this to the fact that the TiN layers in the cited study appeared to partially react or break down during the annealing process, leading to a mixed MoSe_2/TiN back contact rather than a pure TiN one as in the present case.

While the poorer electrical characteristics of the TiN/CZTS contact should be borne in mind when comparing the rest of the devices in this study, we shall shortly see that this can easily be separated from larger differences arising as a result of changing anneal conditions.

Part II: Effects of Back Contact Reactions on Device Properties. We now come to the central aim of this investigation, which is to determine the effect of back contact stability during annealing on the final device performance. To do this, we compare samples with and without the TiN barrier under different annealing conditions, in which the main variables are the effective S and SnS partial pressures experienced at the film surface, and in the presence or absence of a supply of excess S. In the following, we first describe in detail the expected differences in surface and back contact chemistry for the samples A–F and then compare their device characteristics with reference to these differences.

Samples A and B are the “baseline” samples. They were annealed with added elemental S in a small graphite box, so they experienced a high pressure of S during annealing. In addition, the graphite box used for annealing is saturated with SnS because of repeated usage (this has been determined by EDS measurements on the interior walls of the box). Therefore, both samples’ surfaces should have been chemically stabilized against the surface decomposition reactions discussed earlier. Their back contacts were also stabilized but for different reasons: in sample A because of the rapid formation of a thick ($\sim 60 \text{ nm}$) MoS_2 layer due to the S excess and in sample B because the TiN barrier layer is chemically inert and does not react with the CZTS layer, as shown in the previous section.

Samples C and D were annealed without a supply of excess S but with a glass cover on their surfaces. The glass cover places the surfaces in pseudo-equilibrium during annealing by reducing the rate at which S and SnS vapors from the surface can be lost to the atmosphere. However, the back contact of sample C is unstable because there is no excess supply of S available to form a passivating MoS_2 layer, with the result that the CZTS layer itself reacts with the Mo substrate to form MoS_2 (as seen in Figure 3a). By contrast, this does not occur in sample D because of the presence of the TiN barrier.

Samples E and F were annealed without the glass cover and with no added source of S. Their surfaces were therefore not stabilized against decomposition because any S and SnS vapors were able to escape directly and irreversibly to the free volume of the furnace, allowing the surface decomposition processes to occur at a maximum rate. The back contact conditions for samples E and F were the same as for samples C and D, respectively, i.e., unstable for sample E because of the lack of

external S supply (MoS_2 forming by reaction with the CZTS layer) and stable for sample F because of the TiN barrier layer. Table 2 summarizes the above discussion by indicating whether the surfaces and back contacts were stable or not during CZTS synthesis. The sample compositions after annealing are also shown. Table 3 shows device and diode parameters. We emphasize that since all other process steps were identical, the differences in device performance for samples with the same type of back contact can only be due to changes in the CZTS layers as a result of the described chemical differences during annealing.

External quantum efficiency (EQE) and J - V curves for the devices with unmodified Mo back contacts, i.e., A, C, and E, are shown in Figure 5. Comparing the baseline sample A with

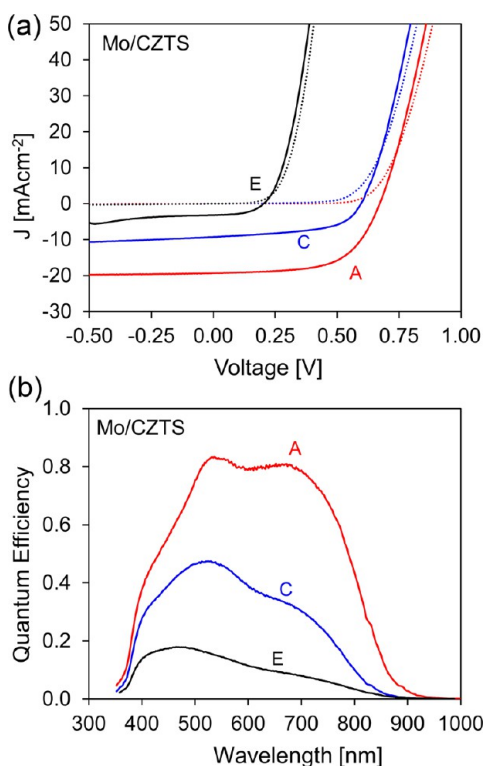


Figure 5. (a) Current–voltage curves and (b) EQE curves for samples A, C, and E, those with normal Mo back contacts (see Tables 2 and 3 for further sample details).

sample C, we see drastic losses in short circuit current density (J_{sc}), from 19.6 to 9.4 mA cm^{-2} and minor losses in open circuit voltage (V_{oc}) and fill factor (FF). The voltage loss is not only due to the reduction in photocurrent density (shown by the fact that the dark J - V curves for the two samples do not coincide); there is also some reduction in diode quality in sample C. The result is an efficiency drop from 7.9% to 3.0%. From the EQE curves for these devices, the current losses in sample C are seen to occur over the entire spectrum, although they are greater for the longer wavelengths. Moving on to sample E, we find large losses in both V_{oc} and J_{sc} . This indicates a large increase in recombination rate, reducing the device efficiency to only 0.3%.

We now consider the samples with the TiN barrier layer (samples B, D, and F), where we must bear in mind the aforementioned nonideality of the back contact and the resulting loss in FF that affects all samples. The device data

are shown in Figure 6. When comparing the baseline annealed sample B with sample D, where a glass cover was used to

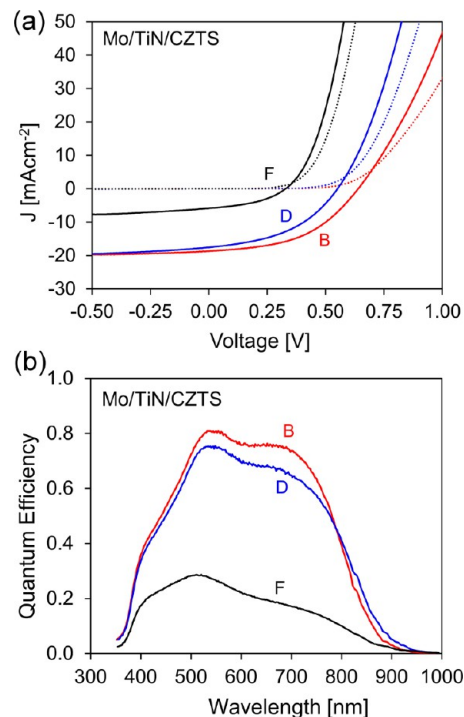


Figure 6. (a) Current–voltage curves and (b) EQE curves for samples B, D, and F, those with TiN-passivated Mo back contacts (see Tables 2 and 3 for further sample details).

protect the surface during annealing, we see a clear distinction from the case without the barrier layer. Whereas the sample with the unmodified back contact (sample C) had a large reduction in short circuit current density compared to the S-annealed baseline, the sample with the TiN barrier layer did not; in fact the short circuit current density for sample D is only fractionally smaller than that of sample B. Overall, despite the poorer electrical properties of the TiN back contact, sample D had a *higher* efficiency than sample C.

In sample F, when there is no glass cover on the sample surface and no added S, we again find the large current losses seen for samples C and E, accompanied now by a large drop in open circuit voltage.

We note that samples C and D had nearly identical voltage losses (71 and 70 mV, respectively) compared to their S-annealed references A and B. The similarity suggests that the voltage losses were related to the differences in annealing condition, independent of the type of back contact. We return to this later.

Without making any assumptions, one can clearly distinguish two separate performance-limiting effects from the device data for samples A–F:

- (1) In samples where the *surface* of the CZTS film was unstable during annealing, large J_{sc} and V_{oc} losses occurred.
- (2) In samples where the *back contact* of the CZTS film was unstable during annealing, large J_{sc} losses occurred without associated V_{oc} losses.

In other words, *both* the *surface and back contact* conditions during annealing (or general thermal processing) are important

for achieving efficient CZTS devices. An unstable back contact yields reduced J_{sc} in the final device, while an unstable surface causes losses of both J_{sc} and V_{oc} . If only one or the other interface is stable (samples C and F), there is still severe degradation to the cell performance. While the importance of surface stability was already known, this is the first experimental demonstration of the importance of the back contact chemistry in determining the electrical quality of CZTS layers. Of course, the presence of separate detrimental processes associated with the surface and back contact conditions, respectively, accords exactly with the picture of separate chemical reactions occurring at these interfaces, as outlined in the Introduction. The detailed agreement between the chemical picture and the changes in device performance is now discussed.

The reactions described in the Introduction (and Table 1) show that both the surface and back contact reactions are suppressed by the presence of S vapor. However, there are some essential differences in the suppression mechanism that are also reflected in the devices in this study, as we now describe. The device losses associated with the sample surface were almost entirely avoided by placing a glass cover on the samples during annealing, i.e., by restricting the free volume above the sample. At equilibrium, the pressure of S and SnS generated from reaction 1 above the CZTS surface (i.e., in the very narrow space between the CZTS film and the glass cover) should be in the range 10^{-3} – 10^{-4} mbar at 550 °C.¹³ In such a small space, this pressure could be generated with minimal surface decomposition. Thus, the expectation from the chemical viewpoint is that a glass cover should effectively prevent surface decomposition, and indeed the device results show that this anneal method does considerably reduce performance losses. The ~70 mV loss in V_{oc} when annealing with this configuration could be explained by the fact that the equilibrium is not perfect: the cover does not form a closed system, and S and SnS vapor can of course escape at the edges. This acts as a drain on the stabilizing atmosphere under the cover, which would cause a continual, albeit slow, surface decomposition. Even so, the glass cover prevented 80–90% of the voltage and current losses that occur in the absence of any form of surface protection (comparing devices B, D, and F).

In contrast, the performance loss associated with the back contact was only avoided by providing a supply of *excess* S (sample A) or by the presence of the TiN barrier (samples B and D). This also agrees with the chemical picture. Unlike the surface reactions, the back contact reactions do not have any equilibrium condition: they will only be suppressed once an effective barrier is interposed between Mo and CZTS to block diffusion of S atoms. We have two such layers in this study, MoS₂, which grows during the process, and TiN, added deliberately. MoS₂ appears to be a poor diffusion barrier, since it easily grows to a considerable thickness, implying continuous diffusion of S atoms across it. Thus, a very thick MoS₂ layer is needed to stop the back contact reactions, which requires a large amount of S to be available. This was the case for sample A: the presence of a large S pressure provided a constant supply of S atoms for growth of MoS₂. In general, the faster the MoS₂ layer grows and the thicker it gets, the more effectively the back contact reactions will be suppressed, so the higher is the S pressure, the better. In the absence of an external source of S, reactions 4–6 in Table 1 can operate, and MoS₂ will grow at the expense of the CZTS layer. On the other hand, a 20 nm TiN layer is, as we showed, a very effective diffusion barrier to S atoms, and so no external supply of S is required to prevent the

back contact reactions. Mirroring the chemical picture, the absence of excess S caused large losses in sample C (unmodified back contact), but these were almost completely avoided in sample D (TiN-passivated back contact).

This detailed agreement between the results of the annealing experiments and the expectations from the chemical reactions supports the hypothesis that the chemical reactions at the two interfaces of the CZTS are the cause of the differences in device performance for samples A–F. Final proof of this hypothesis will be discussed in the next section. In the meantime, it is interesting to ask how the described differences in the suppression mechanisms of the surface and back contact processes affect the synthesis methods used for CZTS and, more generally, CZTS(e). As discussed, the best CZTS(e) devices to date are typically prepared using high S(e) pressures during annealing, of the order of tens to hundreds of mbar in S(e) pressure (e.g., see ref 5). It was previously supposed that the need for such high S(e) pressure arose because of the *surface* decomposition reactions (i.e., S(e) and SnS(e) loss).¹³ However, there is an obvious mismatch between the mentioned experimental values of S(e) pressure and the theoretical equilibrium S(e) pressure needed to prevent surface decomposition (2×10^{-4} mbar for S, with a saturated SnS atmosphere¹³). The new results clarify the situation by showing that the greater part of the required S(e) pressure is in fact needed to stabilize the Mo back contact, by formation of a MoS(e)₂ layer. The conclusion from this is that if we instead stabilize the back contact by another means, for example, by using an appropriate barrier layer, then the requirement for high S(e) pressure should be removed. The remaining requirement, which is to create equilibrium at the CZTS(e) surface, is much easier to satisfy. This insight could allow for much greater flexibility and reduced complexity in CZTS(e) synthesis processes. The TiN-passivated back contact is one possible method of stabilizing the back contact without needing a large S(e) pressure, although the electrical properties of this particular contact need to be improved. Regarding the latter point, more detailed electrical measurements of the interfaces formed between CZTS(e) and different inert materials (e.g., other transition metal nitrides) would be valuable to determine the source of the series resistance and identify methods to improve the back contact.

Part III: Materials Characterization. A final proof that the reactions in Table 1 are the true origin of the losses in device performance requires observation of the products that connect the chemical reactions with the electrical effects. These could be defects, secondary phases, or other inhomogeneities. The current losses in devices C, E, and F are consistent with a “dead area” phenomenon, i.e., regions of the absorber layer that make no contribution to the overall current from the film. Therefore, one suggestion is that insulating secondary phases, such as ZnS produced by the reactions, accumulated at the interfaces and caused current blocking in samples C, E, and F (e.g., see ref 23). Another cause of reduced device performance could be point defects generated in the CZTS layer by the reactions. It has in fact been observed that the density of deep defects in CZTSe depends on selenium pressure during postannealing,⁵ providing a possible link to the surface chemistry. Unfortunately, detection of small quantities of secondary phases, especially confined to interfaces, is difficult for various reasons (e.g., overlapping signals in XRD and Raman, a small interaction volume, etc.) and is even more complicated if the CZTS films are nonstoichiometric. As for point defects, even if

defect energy levels can be detected, assigning them to a particular defect type and determining the origin of this defect are extremely difficult. Accordingly, while we find some interesting differences between samples A–F in the materials characterization, we cannot conclusively determine the reasons for device performance differences. We include the main results here for the sake of completeness.

First, considering the EDS compositions of samples A–F after annealing, the clearest trend is in the Cu/Sn ratio, which in all samples increases from 1.9 in the precursor to 2.0 in the annealed film. There are two possible contributions to this change, namely, (a) loss of Sn from the sample in the form of SnS and (b) accumulation of Sn-containing phases toward the back contact, i.e., beyond the information depth of EDS. Since the changes in Cu/Sn ratio apparently stop at exactly 2.0, we can conclude that the measurable changes came *mainly* from loss or migration of the *excess* Sn content rather than loss from the bulk CZTS phase. Of course, losses from the bulk phase of less than a few atomic percent would not be detectable by EDS (but could still affect the interface properties). In all samples apart from sample E, the Cu/Zn ratio increased from 1.8 to 1.9 during annealing. This could be explained by accumulation of Zn(S) toward the back contact.

SEM cross sections of the completed devices (Figure 7) revealed that the morphology of the CZTS layer was influenced

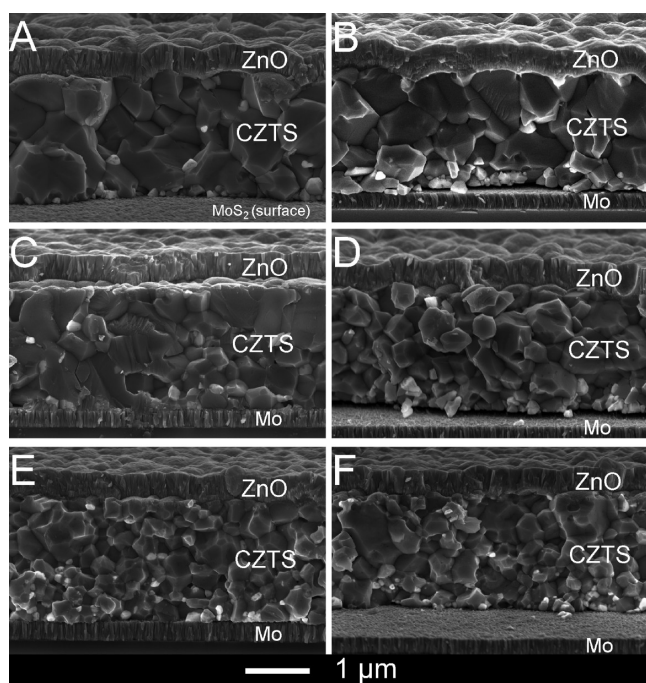


Figure 7. Cross-sectional SEM images taken from finished devices processed from samples A–F. See Table 2 for further sample details.

by the anneal method but not by the type of back contact. The largest grains were seen in samples A and B, those annealed with excess S, and the smallest grains were seen in samples E and F. These variations could be attributable to differences in the temperature due to the changes in anneal configuration. The smaller, brighter particles are most likely to be ZnS, based on our experience of similar samples with higher Zn content or sputtered pure ZnS layers. The greater density of these particles nearer the back contact is consistent with the apparent decrease

in Zn content measured by EDS after annealing and with the SIMS data.

Surface analysis using Raman scattering at an excitation wavelength of 514 nm again revealed no significant differences between the samples, as shown in Figure 8 (for clarity, only

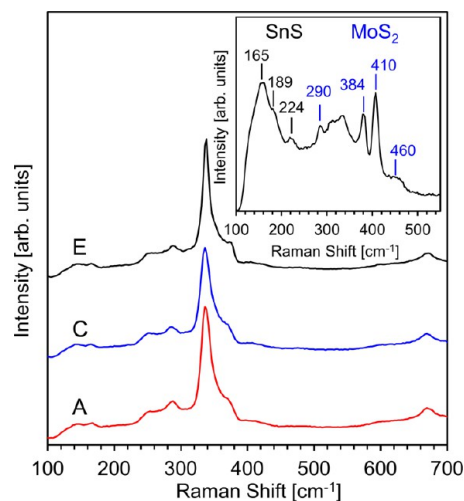


Figure 8. Surface Raman scattering spectra of samples A, C, and E. Inset: spectra recorded on the substrate of sample A after lift-off of the CZTS film, where large inhomogeneities could be seen in the optical microscope.

samples A, C, and E are shown), and only peaks corresponding to CZTS were seen.²⁴ While Sn–S phases and CuS would be observable in this setup, ZnS gives very low intensity due to its weak absorption at 514 nm, and Cu_{2-x}S gives very low intensity due to its metallic character.²⁵ We performed a “lift-off” procedure on the samples and used Raman scattering to examine the exposed substrates and back surfaces of the CZTS films in more detail. Large inhomogeneities appearing at regular intervals could be seen in the optical microscope of the Raman system in samples A and B, which were large enough (several tens of micrometers) to be identified by Raman. This is shown in the inset to Figure 8; the broad peaks at 165, 189, and 224 cm⁻¹ reveal the presence of SnS.²⁶ On the basis of the optical images (not shown), the coverage of the back surface by SnS regions was estimated to be around 20% for sample A and 10% for sample B. In samples C–F, similar-looking regions were seen, although they were too small to yield a reliable Raman spectrum. To examine these regions in more detail, we performed EDS mapping of the back surfaces of the CZTS films. Representative EDS maps are shown in Figure 9. We see segregations of Zn- and Sn-rich material at the back contact in all samples. Note that the large Sn-rich regions in samples A and B are not shown in these images in order to more clearly reveal the structure of the Zn-rich regions. The Zn-rich regions segregated in a similar way independent of anneal condition or back contact material, forming a network on a length scale of around 0.2–0.5 μm. This likely corresponds to the ZnS particles observed in SEM cross sections. These segregations could account for part or all of the apparent change in composition seen by EDS. The segregations of Sn-rich material showed more variation among the samples: the segregated regions are largest in samples A and B and smallest in samples E and F, and their coverage of the back contact region was 2–3 times greater for the samples with unmodified Mo back

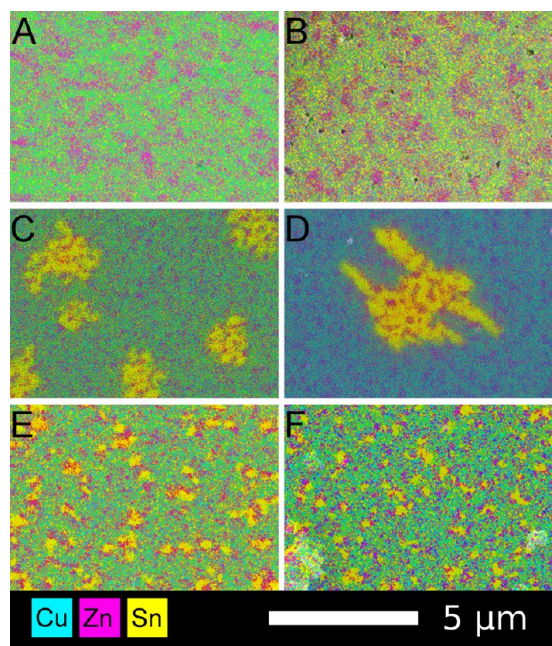


Figure 9. EDS maps (color) of the back surfaces of the CZTS films (A–F) after lift-off. See Table 2 for further sample details.

contacts compared to those with TiN barrier layers. Similar mapping experiments of the CZTS top surfaces revealed no composition segregations at the level of detail possible with the EDS probe.

The segregation of Zn- and Sn-rich regions at the back contacts is the most interesting feature in this sample series. There are several possible contributions to this segregation. The first is spontaneous precipitation of the precursors' excess Sn and Zn content to allow formation of a stoichiometric bulk phase (the Cu/Sn ratio in the precursor was 1.9, and the Cu/Zn ratio was 1.8). There could also be a contribution from the back contact decomposition reactions discussed in the introduction to this paper. However, since these reactions apparently do not occur in the samples with the TiN barrier (i.e., MoS₂ was not observed), the latter explanation cannot account for the larger part of the observed secondary phases in samples B, D, and F, and the former explanation is thus the more likely one. Nonetheless, the consistent increase in coverage of the back contact by Sn-rich material in the samples on Mo (samples A, C, and E) compared to those on TiN could be evidence of a decomposition reaction occurring *in addition* to the segregation of Sn and Zn excess in those samples.

The “dead area” phenomenon with which we tentatively explained the current losses in devices C, E, and F does not have any clear origin in the morphology of the samples. While the Sn- and Zn-rich segregations seen in Figure 9 could be argued to cause dead area, these features obviously cannot be the main cause of the current losses, since similar segregations were seen in all samples (despite some variations of degree and length scale), whereas the current losses only occurred in certain samples. In addition, no such segregations were seen at the CZTS film surfaces, leaving us with no clear cause for the observed current losses associated with unstable surface conditions (in samples E and F). It appears that the real causes of the performance variations for the devices in this study are on a smaller scale than we were able to observe here, in other words, secondary phases with a dimension smaller than

around 50–100 nm and/or point defects in the CZTS phase. To shed more light on the changes in device performance, the front and back interfaces need to be probed in even greater detail.

CONCLUSIONS

The purpose of this study was to discover whether the previously determined chemical reactions between CZTS absorber layers and the normal Mo back contact had any effect on device performance. By combining modifications of the back contact with variations in the annealing conditions, we were able to show that there is indeed a strong correlation between the chemical picture and the variations in device performance. On the basis of this, we proposed that the need for high S(e) pressures during preparation of CZTS(e) absorber layers not only is due to the surface decomposition (commonly referred to as “Sn loss”) but is in fact strongly influenced by the back contact chemistry. The development of an inert back contact based on TiN-passivated Mo was a crucial step in this study because it enabled us to separate the effects of surface and back contact annealing chemistry on the final CZTS devices. Regarding the TiN back contact, we extended on the previous work in several ways. We showed that a TiN barrier layer can indeed passivate interface reactions between Mo and the CZTS layer, as well as those between the Mo and S from the annealing atmosphere, but Na transport from the substrate is not affected. Unfortunately, the TiN/CZTS contact induces a rather high series resistance in the device. Therefore, further work is needed to develop inert back contacts with better electrical characteristics. If this were achieved, it could enable CZTS(e) synthesis processes using much lower chalcogen pressures, giving more flexibility and less complicated synthesis.

Definite proof of the connection between the chemical reactions and the changes in device performance was attempted, but even rather detailed materials characterization was not able to resolve the particular chemical products that led to the large differences in device performance. The devices in this study varied from 0.3% to 7.9% efficient, but no strong differences were observed by Raman, SEM, or EDS mapping at the surfaces and back contacts. This means that the causes of the electrical differences are on a smaller scale than the resolution of these techniques and could be, for example, very finely distributed secondary phases, changes in grain boundaries, or of course, point defects. Despite these unknowns, this study enabled us to identify routes to improving material and device quality, as well as providing some direction for further studies of loss mechanisms in CZTS solar cells. This will be vital information in the effort to improve the efficiency of these devices.

AUTHOR INFORMATION

Notes

The authors declare no competing financial interest.

ACKNOWLEDGMENTS

This work was funded by the Göran Gustafsson Foundation, the Swedish Energy Agency, and the Swedish Research Council.

■ ADDITIONAL NOTE

^aWe also consider the coevaporation process employed in ref 6 as a two-stage process, since an in situ anneal in Sn and Se vapor is performed as a critical step after the main part of film deposition.

■ REFERENCES

- (1) Todorov, T. K.; Tang, J.; Bag, S.; Gunawan, O.; Gokmen, T.; Zhu, Y.; Mitzi, D. B. *Adv. Energy Mater.* **2013**, *3*, 34.
- (2) Mitzi, D. B.; Gunawan, O.; Todorov, T. K.; Wang, K.; Guha, S. *Sol. Energy Mater. Sol. Cells* **2011**, *95*.
- (3) Wang, H. *Int. J. Photoenergy* **2011**, 801292, DOI: 10.1155/2011/801292.
- (4) Shin, B.; Gunawan, O.; Zhu, Y.; Bojarczuk, N. A.; Chey, S. J.; Guha, S. *Prog. Photovolt. Res. Appl.* **2013**, *21*, 72.
- (5) Shin, B.; Zhu, Y.; Bojarczuk, N. A.; Chey, S. J.; Guha, S. *Appl. Phys. Lett.* **2012**, *101*, 053903.
- (6) Repins, I.; Beall, C.; Vora, N.; DeHart, C.; Kuciauskas, D.; Dippo, P.; To, B.; Mann, J.; Hsu, W.-C.; Goodrich, A.; Noufi, R. *Sol. Energy Mater. Sol. Cells* **2012**, *101*, 154.
- (7) Kato, T.; Hiroi, H.; Sakai, N.; Muraoka, S.; Sugimoto, H. *Proceedings of the 27th European Photovoltaic Solar Energy Conference and Exhibition*, Frankfurt, Germany, 2012; EU PVSEC, 2012; p 2236.
- (8) Redinger, A.; Berg, D. M.; Dale, P. J.; Siebentritt, S. *J. Am. Chem. Soc.* **2011**, *133*, 3320.
- (9) Weber, A.; Mainz, R.; Schock, H. W. *J. Appl. Phys.* **2010**, 107.
- (10) Piacente, V.; Foglia, S.; Scardala, P. *J. Alloys Compd.* **1991**, *177*, 17.
- (11) Scragg, J. J.; Wätjen, J. T.; Edoff, M.; Ericson, T.; Kubart, T.; Platzer-Björkman, C. *J. Am. Chem. Soc.* **2012**, *134*, 19330.
- (12) Scragg, J. J.; Dale, P. J.; Colombara, D.; Peter, L. M. *ChemPhysChem* **2012**, *13*, 3035.
- (13) Scragg, J. J.; Ericson, T.; Kubart, T.; Edoff, M.; Platzer-Björkman, C. *Chem. Mater.* **2011**, *23*, 4625.
- (14) Lindahl, J.; Zimmermann, U.; Szaniawski, P.; Torndahl, T.; Hultqvist, A.; Salome, P.; Platzer-Björkman, C.; Edoff, M. *IEEE J. Photovoltaics* **2013**, *1*.
- (15) Ericson, T.; Kubart, T.; Scragg, J. J.; Platzer-Björkman, C. *Thin Solid Films* **2012**, *520*, 7093.
- (16) Scragg, J. J.; Ericson, T.; Fontané, X.; Izquierdo-Roca, V.; Pérez-Rodríguez, A.; Kubart, T.; Edoff, M.; Platzer-Björkman, C. *Prog. Photovoltaics: Res. Appl.* [Online early access]. DOI: 10.1002/pip.2265. Published Online: July 10, 2012.
- (17) Olekseyuk, I. D.; Dudchak, I. V.; Piskach, L. V. *J. Alloys Compd.* **2004**, *368*, 135.
- (18) Westlinder, J.; Sjöblom, G.; Olsson, J. *Microelectron. Eng.* **2004**, *75* (4), 389–396.
- (19) Constable, C. P.; Yarwood, J.; Münz, W.-D. *Surf. Coat. Technol.* **1999**, *116–119*, 155–159.
- (20) Sandoval, S. J.; Yang, D.; Frindt, R. F.; Irwin, J. C. *Phys. Rev. B* **1991**, *44*, 3955.
- (21) Hegedus, S. S.; Shafarman, W. N. *Prog. Photovoltaics: Res. Appl.* **2004**, *12*, 155.
- (22) Malmstrom, J.; Schleussner, S.; Stolt, L. *Appl. Phys. Lett.* **2004**, *85*, 2634.
- (23) Wätjen, J. T.; Engman, J.; Edoff, M.; Platzer-Björkman, C. *Appl. Phys. Lett.* **2012**, *100*, 173510.
- (24) Fontane, X.; Calvo-Barrio, L.; Izquierdo-Roca, V.; Saucedo, E.; Pérez-Rodríguez, A.; Morante, J. R.; Berg, D. M.; Dale, P. J.; Siebentritt, S. *Appl. Phys. Lett.* **2011**, *98*, 181905.
- (25) Munce, C. G.; Parker, G. K.; Holt, S. A.; Hope, G. A. *Colloids Surf., A* **2007**, *295*, 152.
- (26) Parkin, I. P.; Price, L. S.; Hibbert, T. G.; Molloy, K. C. *J. Mater. Chem.* **2001**, *11*, 1486.